Results in Physics 64 (2024) 107932

Contents lists available at ScienceDirect

Results in Physics

journal homepage: www.elsevier.com/locate/rinp

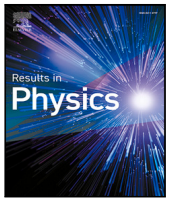

Asymmetric diffraction in anti-parity-time symmetry of non-Hermitian photonic lattice

Runrun Li [a,b], Hengfei Zhang [a,b], Jinpeng Yuan [a,b,*], Lirong Wang [a,b,*], Liantuan Xiao [a,b], Suotang Jia [a,b]

[a] State Key Laboratory of Quantum Optics and Quantum Optics Devices, Institute of Laser Spectroscopy, Shanxi University, 92 Wucheng Road, Taiyuan 030006, China

[b] Collaborative Innovation Center of Extreme Optics, Shanxi University, 92 Wucheng Road, Taiyuan 030006, China

ARTICLE INFO

Keywords:
Asymmetric diffraction
Anti-parity-time symmetry
Non-Hermitian photonic lattice

ABSTRACT

Non-Hermitian systems based on anti-parity-time (PT) symmetry reveal rich physics beyond the Hermitian regime. Here, the anti-PT-symmetric photonic lattice is effectively achieved in a four-level inverted Y-type ^{85}Rb atomic vapor. Such instantaneously reconfigurable anti-PT-symmetric photonic lattice possessing susceptibility of $\chi(x) = -\chi^*(-x)$, is established by a one-dimensional standing-wave coupling field under the assist of a standing-wave driving field. The input probe beam experiences a periodic refractive index modulation when traveling through the photonic lattice, the evolution of output diffraction patterns with symmetric, asymmetric, and lopsided intensity distribution is obtained by adjusting the relevant parameters of constructed non-Hermitian system. Moreover, the anti-PT symmetry in two-dimensional case of both square and hexagonal lattices are correspondingly realized. Our work promotes the development of non-Hermitian devices, and also has some important applications in quantum simulation.

Introduction

Parity-time (PT) symmetry, which Hamiltonian satisfies the commutation relation $[H, PT] = 0$, are fruitful in many areas such as acoustics [1,2], quantum field theory [3], and electronics [4] since it shows the non-Hermitian Hamiltonian operator can exhibit entirely real spectra [5]. In recent years, PT symmetry has been extended to the field of optics by exploiting the mathematical isomorphism existing between the quantum Schrödinger's equation and the paraxial wave equation [6,7]. In optical systems, PT symmetry can be easily established by efficiently combining gain and loss, that is, the refractive index is equivalent to complex potential role in quantum mechanics [8]. Based on this unique property, numerous optical PT-symmetric systems have been theoretically and experimentally realized in synthetic waveguides [9], coherent perfect absorbers [10], microcavities [11], and cold-atom gases [12,13]. Meanwhile, many novel optical phenomena have been discovered, such as Bloch oscillation [14], single-mode laser [15], unidirectional light propagation [16,17], spectral singularity [18], and asymmetric Bragg diffraction [19].

With the deepening of research on non-Hermitian PT symmetry, another non-Hermitian system, anti-PT symmetry, has attracted significant attention in selective mode amplification [20], optical energy-difference conservation [21], and nonlinear crystals [22,23]. In contrast to the condition of the PT-symmetric Hamiltonian, the anti-PT symmetry requires the non-Hermitian Hamiltonian to be anti-commutative with the PT operator, i.e., $\{H, PT\} = 0$, and the eigenvalues of the Hamiltonian of anti-PT-symmetric systems are purely imaginary [24]. Therefore, the anti-PT-symmetric system satisfies the complex refractive index condition $n(x) = -n^*(-x)$, which means that the real part of the refractive index must be an odd function of x (i.e., $n_r(x) = -n_r(-x)$), while the imaginary part must be an even function of x (i.e., $n_I(x) = n_I(-x)$) [25,26]. Since the first realization of anti-PT-symmetric photonic structures with balanced positive and negative index materials, spontaneous phase transition of the scattering matrix, bidirectional invisibility, and a continuous lasing spectrum have been observed in the optical system [27]. Additionally, the study of anti-PT-symmetric optical systems has been extended to optical fibers [28], coupled waveguides [29], and microcavity [30], leading to the realization of diversified novel optical phenomena, such as lopsided Raman–Nath diffraction [31], unidirectional reflectionless anti-PT-symmetric phenomenon [32], spectral singularities [33], and asymmetric light scattering [34].

A coherently prepared multilevel atomic medium is a qualified candidate for the study of optical PT symmetry and anti-PT symmetry

* Corresponding authors at: State Key Laboratory of Quantum Optics and Quantum Optics Devices, Institute of Laser Spectroscopy, Shanxi University, 92 Wucheng Road, Taiyuan 030006, China.

E-mail addresses: yjp@sxu.edu.cn (J. Yuan), wlr@sxu.edu.cn (L. Wang).

https://doi.org/10.1016/j.rinp.2024.107932
Received 17 May 2024; Received in revised form 16 August 2024; Accepted 20 August 2024
Available online 22 August 2024

because of its easy configuration, flexible tunability, and especially the various coherence control techniques enabled by electromagnetically induced transparency (EIT) [35–37]. Furthermore, the standing-wave field replacing the traveling wave field of EIT can modulate the refractive index, the gain-absorption coefficient, or the spatial distribution of the atomic media to form a photonic lattice [38–40]. In recent years, numerous compelling theoretical mechanisms for achieving PT symmetry have been proposed in atomic medium. The lopsided Raman–Nath diffraction was realized in one-dimensional (1D) and two-dimensional (2D) photonic lattices with periodic PT-symmetric refractive index theoretically in three-level Λ-type [41] and four-level N-type structures [42]. An all-optical-control scheme can simultaneously realize PT-symmetric susceptibilities along the propagation direction of beam by applying an external magnetic field [43]. And the PT symmetry and a lopsided optical diffraction can be realized just with the combination of single spatially periodic modulation and loop-phase [6]. The above theoretical studies predominantly focus on lopsided diffraction, however, the transition process from symmetric to lopsided diffraction in nontrivial photonic lattice, especially the asymmetric diffraction in this process, have not yet been theoretically explored to the best of our knowledge.

In this work, a four-level inverted Y-type ^{85}Rb atomic system is utilized to realize a non-Hermitian anti-PT-symmetric photonic lattice under the condition of EIT. Here, the non-Hermitian system has an anti-PT-symmetric Hamiltonian being anti-commutative with the PT operator ($\{H, PT\} = 0$). Moreover, the probe beam passing through the nontrivial lattice demonstrates several intriguing optical properties, including symmetric diffraction, asymmetric diffraction and lopsided diffraction. When the real part of the refractive index is an even or odd function, it corresponds to symmetric and lopsided diffraction. As the real part of the refractive index deviates from being strictly even or odd functions, the diffraction pattern becomes complex, leading to asymmetric diffraction. Last but not least, by adjusting the relevant parameters, the anti-PT symmetry of the square and the hexagonal lattices are theoretically obtained in 2D case. Due to the highly controllable nature of the system, it offers a platform for exploring non-Hermitian physics within a coherent atomic system. In addition, the far-field diffraction patterns of proposed lattice are focused in our work, the Talbot effect in near-field of PT- or anti-PT-symmetric photonic lattices can further promote the rapid development of light field regulation, which is the great significance for further investigation of simulations and applications based on the electromagnetically induced Talbot effect [44].

Model and equations

Taking ^{85}Rb atoms for the realization of an anti-PT-symmetric photonic lattice, a four-level inverted Y-type atomic system is schematically depicted in Fig. 1(a). A weak probe field E_p with Rabi frequency $\Omega_p = \overrightarrow{\mu_{13}} \cdot \overrightarrow{e_p} E_p/2\hbar$ resonates to the transition $|1\rangle \rightarrow |3\rangle$. The standing-wave coupling field E_c with Rabi frequency $\Omega_c = \overrightarrow{\mu_{34}} \cdot \overrightarrow{e_c} E_c/2\hbar$ stimulates the transition $|3\rangle \rightarrow |4\rangle$, while the transition $|2\rangle \rightarrow |3\rangle$ is driven by a standing-wave driving field E_d with Rabi frequency $\Omega_d = \overrightarrow{\mu_{23}} \cdot \overrightarrow{e_d} E_d/2\hbar$, where $\mu_{ij}(i, j = 1, 2, 3)$ is the transition dipole momentum between the levels $|i\rangle$ and $|j\rangle$, and $\overrightarrow{e_p}$, $\overrightarrow{e_c}$, $\overrightarrow{e_d}$ represent the unit polarization vectors of the probe, coupling, and driving fields, respectively.

Two coupling beams are symmetrically propagated with respect to the z axis and intersect at the center of the ^{85}Rb cell at a small angle 2φ to establish a standing-wave coupling field along the transverse direction x inside the cell. The lattice constant is $d_c = \lambda_c/(2sin\varphi)$, where λ_c is the wavelength of the coupling laser. Similarly, two driving beams, incident from opposite directions and overlap with coupling field, enter the cell at same angle 2φ to generate gain and loss. The spatial-shift distance between the two light fields is $d_c/5$. In order to construct a nontrivial photonic lattice with asymmetric or lopsided diffraction patterns, the Ω_c and Ω_d are periodically modulated in a 1D configuration [42]

$$\Omega_c(x) = \delta\Omega_c sin[2\pi(x - x_i)/d_c], \tag{1}$$

$$\Omega_d(x) = \Omega_{d0} + \delta\Omega_d sin[2\pi(x - x_i)/d_d], \tag{2}$$

here, Ω_{d0} is a fixed background amplitude, $\delta\Omega_c$ and $\delta\Omega_d$ are modulation amplitudes, d_c and d_d is the lattice constant. The probe beam, characterized by a Gaussian intensity profile, propagates through the nontrivial photonic lattices, as shown in Fig. 1(b). The structure of a 1D lattice is formed by the intersection of two strong coupling fields of the same characters at a small angle φ [see Fig. 1(c_1)]. Similarly, 2D square lattices are established by two orthogonal standing-wave fields induced by the interference of two pairs of coupling laser beams [see Fig. 1(c_2)], and a hexagonal lattice is constructed by three coupling fields interfering with a small angle φ along the z direction under EIT condition [see Fig. 1(c_3)] [39,45]. By properly adjusting the parameters, the parity of the real part of the refractive index changes, which is a crucial requirement for achieving exact anti-PT symmetry in optical systems.

Under the electric-dipole and rotating-wave approximations, the interaction Hamiltonian of the inverted Y-type atomic system is given by

$$H = -\frac{\hbar}{2}\begin{bmatrix} 0 & 0 & \Omega_p & 0 \\ 0 & 2(\Delta_p - \Delta_d) & \Omega_d & 0 \\ \Omega_p & \Omega_d & 2\Delta_p & \Omega_c \\ 0 & 0 & \Omega_c & 2(\Delta_p + \Delta_c) \end{bmatrix}, \tag{3}$$

where $\Delta_p = \omega_p - \omega_{13}$, $\Delta_c = \omega_c - \omega_{34}$, and $\Delta_d = \omega_d - \omega_{23}$ are the detunings of the probe, coupling, and driving fields, respectively. The dynamics of the atomic system can be described by using the density matrix approach as [38]

$$\frac{\partial\rho}{\partial t} = -\frac{i}{\hbar}[H, \rho] + L[\rho(t)], \tag{4}$$

here, the Liouvillian matrix $L[\rho(t)]$ indicating the relaxation by spontaneous decay can be written as

$$L[\rho(t)] = \begin{bmatrix} \Gamma_3\rho_{33} & -\gamma_{12}\rho_{12} & -\gamma_{13}\rho_{13} & -\gamma_{14}\rho_{14} \\ -\gamma_{21}\rho_{21} & \Gamma_3\rho_{33} - \Gamma_2\rho_{22} & -\gamma_{23}\rho_{23} & -\gamma_{24}\rho_{24} \\ -\gamma_{31}\rho_{31} & -\gamma_{32}\rho_{32} & \Gamma_4\rho_{44} - \Gamma_3\rho_{33} & -\gamma_{34}\rho_{34} \\ -\gamma_{41}\rho_{41} & -\gamma_{42}\rho_{42} & -\gamma_{43}\rho_{43} & -\Gamma_4\rho_{44} \end{bmatrix}, \tag{5}$$

where $\Gamma_i(i = 1, 2, 3, 4)$ is the spontaneous-emission decay rate of each energy level, and $\gamma_{ij} = \frac{\Gamma_i + \Gamma_j}{2}(i, j = 1, 2, 3, 4)$ are coherence decay rates between the levels $|i\rangle$ and $|j\rangle$.

From this, the density matrix equations are straightforward to further obtain as following

$$\begin{aligned} \frac{\partial\rho_{12}}{\partial t} &= \frac{i}{2}\left[\Omega_p\rho_{32} - 2(\Delta_p - \Delta_d)\rho_{12} - \Omega_d\rho_{13}\right] - \gamma_{12}\rho_{12} \\ \frac{\partial\rho_{13}}{\partial t} &= \frac{i}{2}\left[\Omega_p\rho_{33} - (\Omega_p\rho_{11} + \Omega_d\rho_{12} + 2\Delta_p\rho_{13} + \Omega_c\rho_{14})\right] - \gamma_{13}\rho_{13} \\ \frac{\partial\rho_{23}}{\partial t} &= \frac{i}{2}\left[-2\Delta_d\rho_{23} + \Omega_d\rho_{33} - (\Omega_p\rho_{21} + \Omega_d\rho_{22} + \Omega_c\rho_{24})\right] - \gamma_{23}\rho_{23} \\ \frac{\partial\rho_{41}}{\partial t} &= \frac{i}{2}\left[\Omega_c\rho_{31} + 2(\Delta_p + \Delta_c)\rho_{41} - \Omega_p\rho_{43}\right] - \gamma_{41}\rho_{41} \\ \frac{\partial\rho_{42}}{\partial t} &= \frac{i}{2}\left[\Omega_c\rho_{32} + 2(\Delta_c + \Delta_d)\rho_{42} - \Omega_d\rho_{43}\right] - \gamma_{42}\rho_{42} \\ \frac{\partial\rho_{43}}{\partial t} &= \frac{i}{2}\left[\Omega_c\rho_{33} + 2\Delta_c\rho_{43} - (\Omega_p\rho_{41} + \Omega_d\rho_{42} + \Omega_c\rho_{44})\right] - \gamma_{43}\rho_{43} \end{aligned}. \tag{6}$$

Therefore, under the weak probe field approximation, the steady-state solution of the density matrix element is

$$\rho_{13} = \frac{-2i(\Delta_p - \Delta_d)(i\gamma_{41} + \Delta_p + \Delta_c)\Omega_p}{i(\Delta_p - \Delta_d)\left[4(-i\gamma_{13} + \Delta_p)(i\gamma_{41} + \Delta_p + \Delta_c - \Omega_c^2)\right] + \left[\gamma_{41} - i(\Delta_p + \Delta_c)\right]\Omega_d^2}. \tag{7}$$

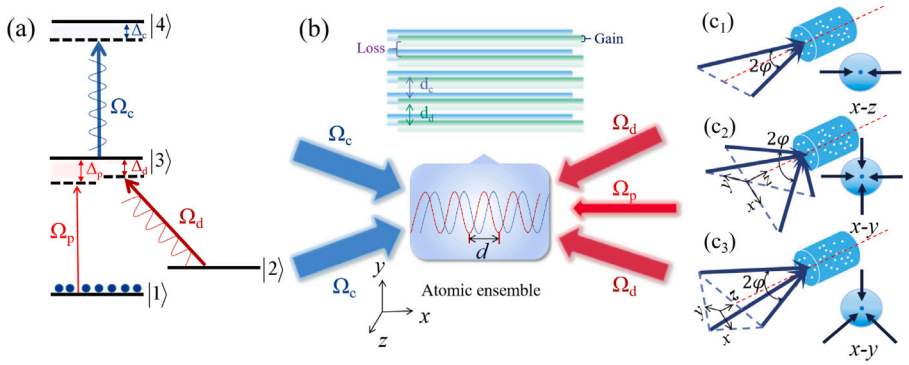

Fig. 1. (a) Energy level diagram of a four-level inverted Y-type atomic system. (b) Diagram of three laser fields interacting with an atomic system. (c_1-c_3) The schematic diagram of generating the periodically modulated 1D lattice, 2D square lattice, and the hexagonal lattice inside the vapor cell.

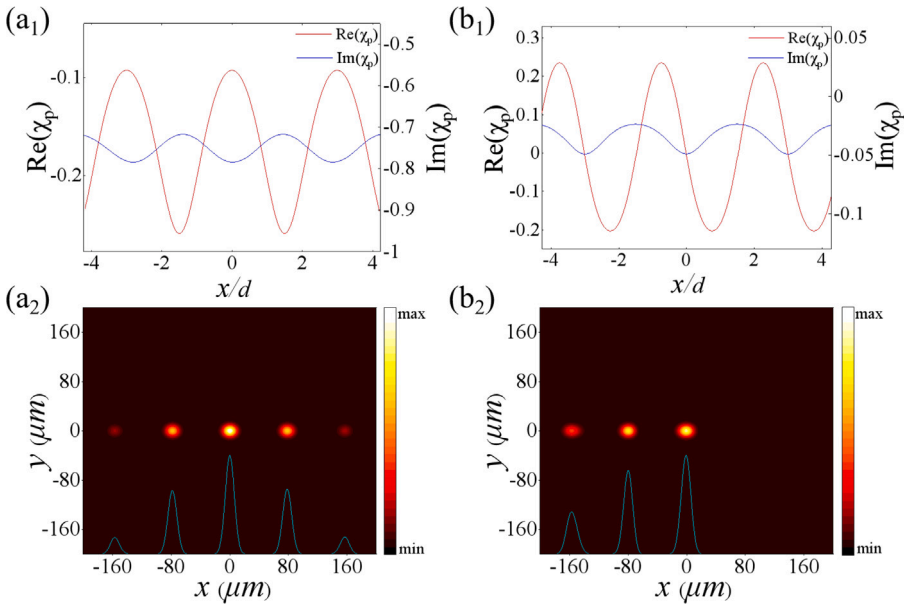

Fig. 2. The real and imaginary parts of susceptibility in a trivial photonic lattice with (a_1) $\Omega_d = 0$, $\Delta_d = 0$ and the nontrivial photonic lattice with (b_1) $\Omega_d = 10$ MHz, $\Delta_d = 6$ MHz. The symmetric diffraction patterns (a_2) and lopsided diffraction patterns (b_2) correspond to (a_1) and (b_1). Other parameters are chosen as $\Omega_p = 2$ MHz, $\Omega_c = 5$ MHz, $\Delta_p = 0$ MHz, $\Delta_c = -6$ MHz, $\Omega_{d0} = 2$ MHz, $\delta\Omega_c = 1$ MHz, and $\delta\Omega_d = 1$ MHz.

The corresponding susceptibility $\chi = \chi' + i\chi''$ is

$$\chi = \frac{N|\mu_{13}|^2}{\hbar\epsilon_0\Omega_p}\rho_{13} = \frac{N|\mu_{13}|^2}{\hbar\epsilon_0} \times \left(-\Delta_p + i\gamma_{13} + \frac{\Omega_d^2/4}{\Delta_p - \Delta_d + i\gamma_{12}} + \frac{\Omega_c^2/4}{\Delta_p + \Delta_c + i\gamma_{41}}\right)^{-1}, \quad (8)$$

where N is the atom number density, ϵ_0 is the permittivity of free space, and μ_{13} is the transition dipole momentum between levels $|1\rangle$ and $|3\rangle$. The real and imaginary parts of the susceptibility are employed to represent the dispersion and absorption characteristics of probe field, respectively. The two terms reflect the degree of interaction between atoms and three laser fields in the four-level atomic system.

The interaction between laser fields and atomic medium can be used to achieve optical anti-PT-symmetric photonic lattice possessing $\chi_p(x,y) = -\chi_p^*(-x,y)$. The relevant refractive index can be obtained via $n_p = \sqrt{1+\chi} \approx 1 + \chi/2$.

The output probe surface at $z = L$ can be expressed as

$$E_p(x,L) = E_p(x,0)exp\left[-\frac{k_p}{2}Im(\chi)L + i\frac{k_p}{2}Re(\chi)L\right], \quad (9)$$

where $E_p(x,0)$ is the input probe profile and $k_p = 2\pi/\lambda_p$, λ_p being the wavelength of the probe field.

By solving Eq. (6), the transmission function of the modulated probe field at $z = L$ can be calculated analytically and is given by

$$T(x,y) = exp\left(-\frac{2\pi L}{\lambda_p}Im(\chi) + i\frac{2\pi L}{\lambda_p}Re(\chi)\right). \quad (10)$$

The amplitude of the far-field diffraction pattern can be expressed as [46]

$$I(x,y) = |\frac{exp(ik_pz)}{i\lambda_pz}exp\left[i\frac{k_p}{2z}(x^2+y^2)\right] \times F\left[E_p(x',y') \times T(x',y')\right]|^2, \quad (11)$$

where F represents the Fourier transform, (x,y) is the coordinate of the field, and (x',y') is the coordinate of the lattice.

Results and discussion

The spatial susceptibility at $\Omega_d = 0$ and $\Delta_d = 0$ is calculated under a three-level cascade systemic EIT condition, and a trivial photonic lattice is realized in Fig. 2(a_1) (i.e., the proposed inverted Y-type atomic system lacks a driving field) [47]. In this case, the real and imaginary parts of the susceptibility are simultaneously even functions of position x, and the corresponding far-field diffraction pattern [according to Eq. (11)] is highly symmetric in positive and negative orders as shown in Fig. 2(a_2). Notably, the introduction of the driving field constructs

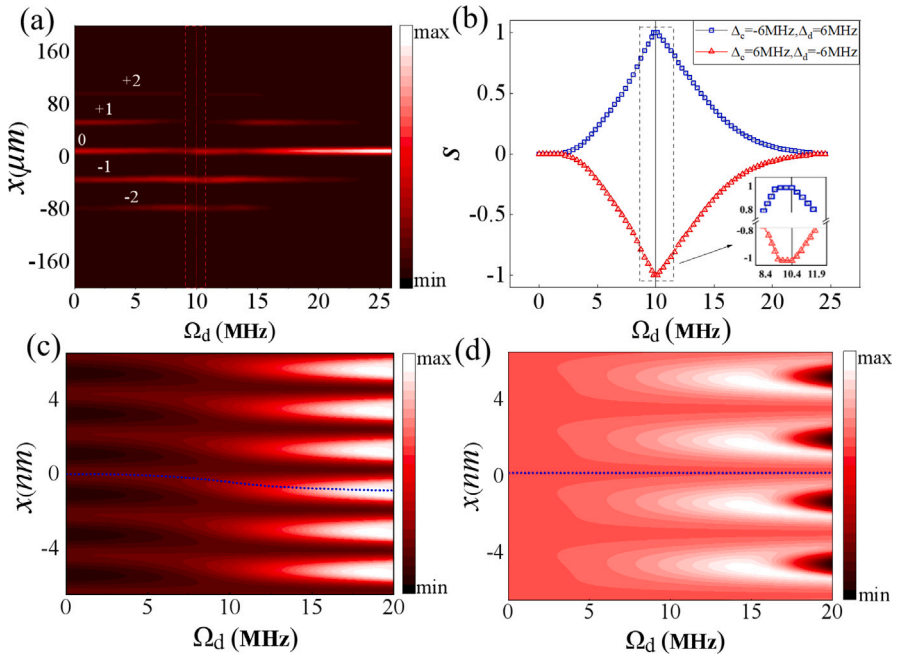

Fig. 3. (a) Normalized diffraction intensity I_p versus the amplitude Ω_d and lattice position x. (b) The variation trend of symmetric parameters and the detail numerical simulations near exceptional point with Ω_d. Here, the other parameters are same as in Fig. 2. (c) The real part and (d) the imaginary part of the refractive index versus the amplitude Ω_d and lattice position x. The other parameters are the same as Fig. 2(b_1).

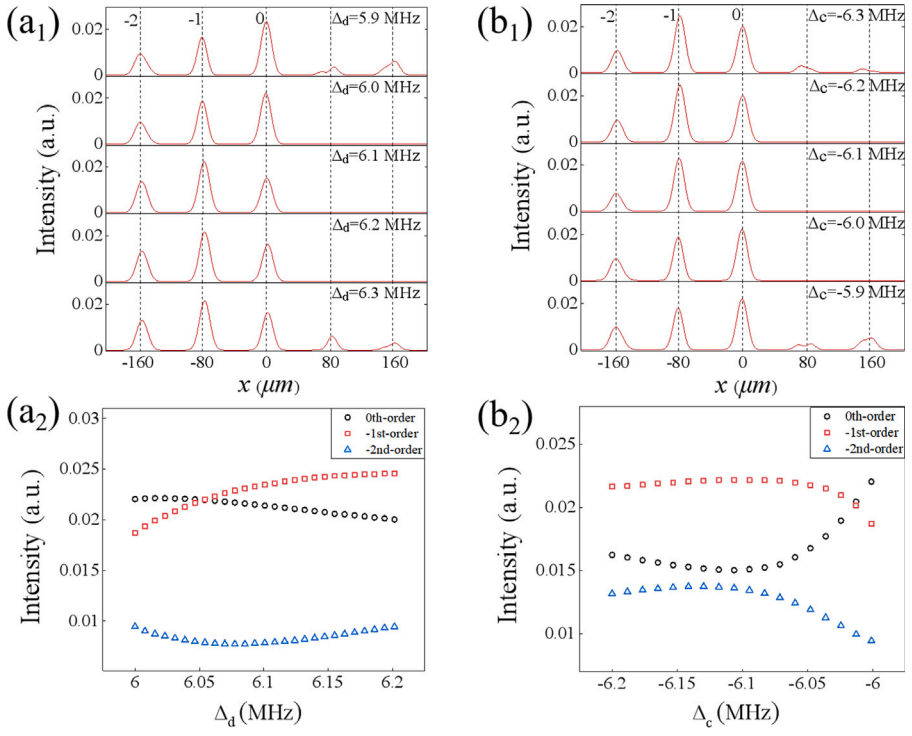

Fig. 4. (a_1-b_1) The influence of the detuning of both two standing-wave fields (Δ_d and Δ_c) on the lopsided diffraction spectra. (a_2-b_2) The intensities of the corresponding 0th, -1st, and -2nd diffraction orders versus detuning Δ_d and Δ_c. The other parameters are the same as Fig. 2(b_1).

a nontrivial photonic lattice. The nontrivial photonic lattice with real (imaginary) part of the susceptibility is odd (even) function of position x is generated under properly adjusting the parameters of $\Omega_d = 10$ MHz and $\Delta_d = 6$ MHz, as shown in Fig. 2(b_1), indicating that an anti-PT-symmetric lattice with $\chi_p(x, y) = -\chi_p^*(-x, y)$ is established. This intriguing lattice is achieved through a precise sinusoidal modulation of standing-wave driving field in terms of intensity (Rabi frequency) or frequency (atom-field detuning) in the inverted Y-type configuration [48,49], and the far-field diffraction of probe field shown in Fig. 2(b_2) exhibits a distinctly lopsided pattern, whose high orders only distributed into the negative range since the anti-PT-symmetric susceptibility corresponds to strongly unbalanced probe reflectivity in the presence of significant loss [50].

The standing-wave driving field plays an important role in transforming a trivial lattice into a nontrivial one. The dependence of the normalized diffraction spectra of photonic lattice to the Rabi frequency Ω_d of driving field is shown in Fig. 3(a) with $\Delta_c = -6$ MHz and $\Delta_d = 6$ MHz. It is evident that there exist a dynamic evolution process involves asymmetric diffraction between the symmetric and lopsided diffractions, which has not been studied in detail. In order to quantitatively demonstrate the occurrence of the anti-PT-symmetric transition, we plot the symmetry parameter obtained from the intensities at two opposite orders for I_{+1} (+1st-order) and I_{-1} (−1st-order). The symmetry parameter written as $S = \frac{I_{+1}-I_{-1}}{I_{+1}+I_{-1}}$, gives $S = 0$ for a trivial lattice with symmetric diffraction and $S = \pm 1$ for a nontrivial lattice with lopsided diffraction. The corresponding symmetry parameter of Fig. 3(a) is shown as the blue dotted line of Fig. 3(b), while the red dotted line in Fig. 3(b) represents the conditions opposite to those depicted by the blue dotted line with respect to $\Delta_c = 6$ MHz and $\Delta_d = -6$ MHz.

The anti-PT-symmetric systems conform to the anti-commutative relations of PT operator, which the anti-PT Hamiltonian is described as [26,51]

$$H = \begin{bmatrix} |\Delta| - i\gamma_{12} & i\Gamma \\ i\Gamma & -|\Delta| - i\gamma_{12} \end{bmatrix}, \tag{12}$$

where $|\Delta| = \left|\Delta_p - \Delta_c\right|$ is the two-photon detuning, $\Gamma = \frac{\Omega_d^2}{\gamma_{23}}$ is the ground-state-coherence coupling rate. Here, $|\Delta| = 6$ MHz, $\gamma_{23} = \pi \times 5.75$ MHz, $\gamma_{12} = 2\pi \times 7.5$ Hz, and $\Omega_c = 5$ MHz.

The eigenvalues of the anti-PT symmetric system can be analytically calculated and expressed as

$$\lambda_{\pm} = -i\gamma_{12} \pm \sqrt{\Delta^2 - \Gamma^2}. \tag{13}$$

When $\Omega_d > 10.4$ MHz (i.e., $|\Delta| < \Gamma$), the eigenvalues of the systems are purely imaginary, which corresponds to anti-PT-symmetric phase. As $\Omega_d = 10.4$ MHz ($|\Delta|/\Gamma \approx 1$), the two eigenmodes degenerate, which corresponds to exceptional point ($|\Delta| = \Gamma$). When Ω_d gradually decreases (corresponding to $|\Delta| > \Gamma$), there exists a transient state of equilibrium, and then the EIT window gradually narrows due to the properties of atomic medium.

As shown in Fig. 3(a) and (b), the diffraction pattern of probe beam keeps symmetrical (i.e., $S = 0$) when $0 \le \Omega_d \le 3.0$ MHz. Such relatively small driving field brings less effects on the characteristics of the original three-level cascade system, and the real part of the refractive index shown in Fig. 3(c) are still even function. The negative orders have a stronger intensity than that in positive when 3.0 MHz $< \Omega_d <$ 10.4 MHz shown in Fig. 3(a), and the corresponding symmetry parameter shown in Fig. 3(b) falls within the range $0 < S < 1$. In this case, the system is gradually close to the anti-PT symmetry. As Ω_d gradually increases, the enhanced driving field induces a nonlinear shift in the real part of the refractive index along the $-x$ direction, making it becomes non-odd and non-even functions, as shown in Fig. 3(c). This change makes the reflection on both sides of the system asymmetrical [42], thereby leading to the asymmetric diffraction of probe beam.

The lopsided diffraction is achieved at 9.6 MHz $\le \Omega_d \le$ 10.4 MHz, where the real parts of the refractive index shift to odd function [see Fig. 3(a) and (c)]. In this case, there is a transient state of equilibrium as shown in the illustration in Fig. 3(b). The corresponding symmetry parameter shown in the blue dot line of Fig. 3(b) reaches the peak of $S = 1$.

With further increasing Ω_d, the eigenvalues of systems are purely imaginary, which corresponds to anti-PT-symmetric phase, the real parts of the refractive index continue undergo nonlinear shift along the $-x$ direction until shift by half a pried to became even functions, this results in S gradually decrease to 0, and the asymmetric diffraction occurs again until it becomes symmetric [see Fig. 3(a–c)]. It is worth mentioning that, the excessive driving field destroys the EIT condition of the system, resulting in the disappearance of higher-order diffraction. In all the above processes, the imaginary part of the refractive index shown in Fig. 3(d) is always an even function, since the anti-PT symmetry is inseparable from the balance optical property, where is associated with the balance of negative dispersion and positive dispersion (i.e., the anti-PT-symmetric system satisfies condition $n(x) = -n^*(-x)$) [27].

The Eq. (8) also reflects that the detunings of laser fields can significantly influence the diffraction intensities of this non-Hermitian photonic lattice. In the following, we investigate the influence of the detuning of both two standing-wave fields (Δ_d and Δ_c) on the lopsided diffraction spectra. As shown in Fig. 4(a_1), the increase of Δ_d stimulates higher-order diffraction fields in the negative-order direction and leads to a redistribution of the diffraction intensities within the negative orders in the lopsided diffraction range of 6.0 MHz $\le \Delta_d \le$ 6.2 MHz, and when Δ_d beyond this range, the anti-PT symmetry will be destroyed, the positive orders appear. Fig. 4(a_2) shows the intensities of the corresponding 0th, -1st, and -2nd diffraction orders as a function of Δ_d. It can be observed that the intensity of −1st order is higher than that of 0th when $\Delta_d \ge 6.1$ MHz. In this case, the phase modulation [$i\frac{2\pi L}{\lambda_p} Re(\chi)$ included in the transmission function of Eq. (10)] becomes dominant in modulating the optical lattice. The phase modulation is a unique characteristic of atomic medium, which disperses energy into higher diffraction orders and distinguishes the photonic lattice from solid material mediums [46,52]. Fig. 4(b_1) and (b_2) show the same as that of Fig. 4(a_1) and (a_2) but as a function of Δ_c. A reversal of the trend of 0th and -1st orders intensities in Fig. 4(b_2) than that in Fig. 4(a_2) is observed, since the effective phase modulation is introduced by detuning the frequencies of laser fields away from the resonance frequency but operates within the EIT window [31].

To demonstrate the universality of the proposed non-Hermitian anti-PT-symmetric photonic lattice, we extend the study from 1D to 2D lattice [39,45]. Fig. 5 shows the diffraction spectra of two kinds typical 2D lattices, square and hexagonal lattices, for different values of Δ_d under proposed non-Hermitian system. When $\Delta_d = 0.5$ MHz, the diffraction spectrum of the 2D lattice is symmetrically distributed across the four quadrants, as shown in Fig. 5(a_1) and (a_2), and the real and imaginary part of the refractive index being even functions. As Δ_d increases to 3 MHz, the real and imaginary parts of the corresponding refractive index are non-odd and non-even functions of the diffraction gradually approaching the first quadrant in Fig. 5(b_1) and (b_2). As shown in Fig. 5(c_1) and (c_2), in the case of $\Delta_d = 5.5$ MHz, the diffraction is concentrated in the first quadrant and lopsided diffraction is realized by the 2D lattices with real (imaginary) part of the susceptibility is odd (even) function. Besides, we can also accurately control the relative intensities of the diffraction fields of the four quadrants via adjusting the other parameters except Δ_d when the probe field passes through the 2D lattices.

Before concluding, an experimental realization of this four-level inverted Y-type atomic system is proposed in ^{85}Rb atomic vapor cell. The suggested states are as follows: $|1\rangle = \left|5S_{1/2}, F = 3\right\rangle$, $|2\rangle = \left|5S_{1/2}, F = 2\right\rangle$, $|3\rangle = \left|5S_{3/2}, F = 2\right\rangle$, and $|4\rangle = \left|5D_{5/2}, F = 1\right\rangle$. To mitigate the Doppler broadening effect in thermal atoms, wherein the probe and coupling (driving) beams are counter- (co-) propagating. The transition of $|1\rangle \rightarrow |3\rangle$ can be stimulated by a weak probe field with wavelength 780.24 nm, while the driving and coupling standing-wave fields with wavelength of 780.03 nm and 776 nm excites the transition of $|2\rangle \rightarrow |3\rangle$ and $|3\rangle \rightarrow |4\rangle$, respectively. The external cavity diode lasers can provide these laser fields that are required for the experiment.

Conclusion

In conclusion, we have theoretically investigated the asymmetric diffraction in an non-Hermitian photonic lattice. The realization of lopsided diffraction in this nontrivial photonic lattice, compared to a

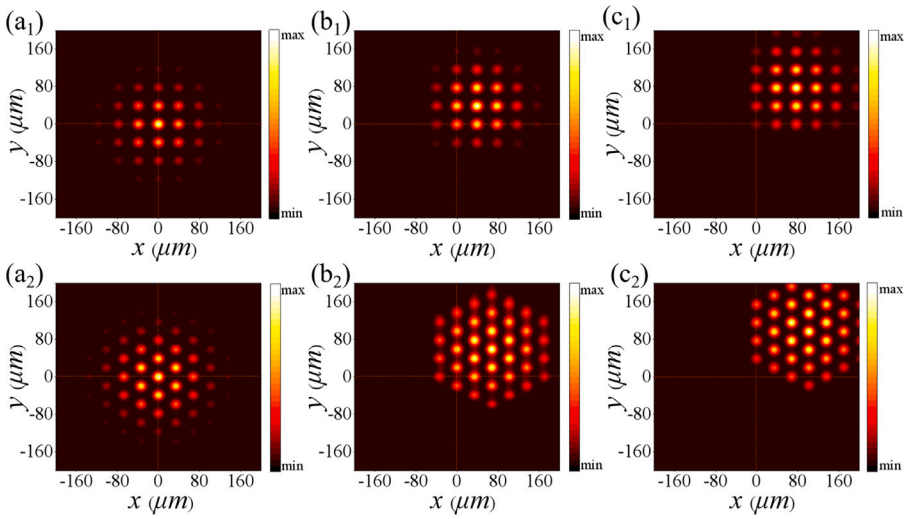

Fig. 5. The two-dimensional diffraction spectra for different Δ_d of square lattice (a_1-c_1) and hexagonal diffraction lattice (a_2-c_2). Here, (a_1-a_2) $\Delta_d = 0.5$ MHz, (b_1-b_2) $\Delta_d = 3$ MHz, (c_1-c_2) $\Delta_d = 5.5$ MHz. The other parameters are the same as Fig. 2(b_1).

trivial photonic lattice, highlights the significant role of the standing-wave driving field in transforming a trivial lattice into a nontrivial one. A dynamic evolution process involves asymmetric diffraction, between the symmetric and lopsided diffraction. With phase modulation being a unique characteristic of atomic medium, which disperses energy into higher diffraction orders and distinguishes the photonic lattice from solid material mediums. The results all show, the parity of the real (imaginary) part of the refractive index is crucial for achieving the anti-PT symmetry of the square and the hexagonal lattices in 2D theoretically, and this can be realized by adjusting the relevant parameters. This work provides a rich tunable experimental platform for the study of versatile non-Hermitian optical devices.

CRediT authorship contribution statement

Runrun Li: Writing – original draft, Investigation, Formal analysis, Data curation, Conceptualization. **Hengfei Zhang:** Writing – review & editing, Formal analysis, Data curation, Conceptualization. **Jinpeng Yuan:** Writing – review & editing, Project administration, Funding acquisition, Formal analysis, Conceptualization. **Lirong Wang:** Writing – review & editing, Supervision, Resources, Funding acquisition, Formal analysis, Conceptualization. **Liantuan Xiao:** Supervision, Resources, Funding acquisition. **Suotang Jia:** Supervision, Resources, Funding acquisition.

Declaration of competing interest

The authors declare that they have no known competing financial interests or personal relationships that could have appeared to influence the work reported in this paper.

Data availability

Data will be made available on request.

Acknowledgments

This work is supported by the Innovation Program for Quantum Science and Technology (2023ZD0300902), the National Natural Science Foundation of China (62075121), the Fund Program for the Scientific Activities of Selected Returned Overseas Professionals in Shanxi Province (2023001), Shanxi Scholarship Council of China (2024-003), the Fund for Postdoctoral Fellowship Program of CPSF (GZC20231510) and the Fund for Shanxi "1331 Project".

References

[1] Shi C, Dubois M, Chen Y, Cheng L, Ramezani H, Wang Y, Zhang X. Accessing the exceptional points of parity-time symmetric acoustics. Nature Commun 2016;7(1):11110.
[2] Zhu X, Ramezani H, Shi C, Zhu J, Zhang X. PT-symmetric acoustics. Phys Rev X 2014;4(3):031042.
[3] Bender CM, Brody DC, Jones HF. Extension of PT-symmetric quantum mechanics to quantum field theory with cubic interaction. Phys Rev D 2004;70(2):025001.
[4] Ramezani H, Christodoulides DN, Kovanis V, Vitebskiy I, Kottos T. PT-symmetric talbot effects. Phys Rev Lett 2012;109(3):033902.
[5] Bender CM, Boettcher S. Real spectra in non-Hermitian Hamiltonians having PT symmetry. Phys Rev Lett 1998;80(24):5243.
[6] Huo D, Hua S, Tian X-D, Liu Y-M. Lopsided optical diffraction in a loop electromagnetically induced grating. Opt Express 2023;31(10):16251–66.
[7] Klaiman S, Günther U, Moiseyev N. Visualization of branch points in PT-symmetric waveguides. Phys Rev Lett 2008;101(8):080402.
[8] Feng L, El-Ganainy R, Ge L. Non-hermitian photonics based on parity–time symmetry. Nat Photonics 2017;11(12):752–62.
[9] Rüter CE, Makris KG, El-Ganainy R, Christodoulides DN, Segev M, Kip D. Observation of parity-time symmetry in optics. Nat Phys 2010;6(3):192–5.
[10] Longhi S. Non-reciprocal transmission in photonic lattices based on unidirectional coherent perfect absorption. Opt Lett 2015;40(7):1278–81.
[11] Chang L, Jiang X, Hua S, Yang C, Wen J, Jiang L, Li G, Wang G, Xiao M. Parity-time symmetry and variable optical isolation in active-passive-coupled microresonators. Nat Photonics 2014;8(7):524–9.
[12] Hang C, Huang G. Weak-light solitons and their active control in a parity-time-symmetric atomic system. Phys Rev A 2015;91(4):043833.
[13] Li Y, Zhang J, Wang Y, Du H, Wu J, Liu W, Mei F, Ma J, Xiao L, Jia S. Atom-optically synthetic gauge fields for a noninteracting bose gas. Light: Sci Appl 2022;11(1):13.
[14] Longhi S. Bloch oscillations in complex crystals with PT symmetry. Phys Rev Lett 2009;103(12):123601.
[15] Feng L, Wong ZJ, Ma R-M, Wang Y, Zhang X. Single-mode laser by parity-time symmetry breaking. Science 2014;346(6212):972–5.
[16] Lin Z, Ramezani H, Eichelkraut T, Kottos T, Cao H, Christodoulides DN. Unidirectional invisibility induced by PT-symmetric periodic structures. Phys Rev Lett 2011;106(21):213901.
[17] Feng L, Ayache M, Huang J, Xu Y-L, Lu M-H, Chen Y-F, Fainman Y, Scherer A. Nonreciprocal light propagation in a silicon photonic circuit. Science 2011;333(6043):729–33.
[18] Zhu X-Y, Xu Y-L, Zou Y, Sun X-C, He C, Lu M-H, Liu X-P, Chen Y-F. Asymmetric diffraction based on a passive parity-time grating. Appl Phys Lett 2016;109(11).
[19] Longhi S. Spectral singularities and bragg scattering in complex crystals. Phys Rev A 2010;81(2):022102.
[20] Antonosyan DA, Solntsev AS, Sukhorukov AA. Parity-time anti-symmetric parametric amplifier. Opt Lett 2015;40(20):4575–8.
[21] Park S, Lee D, Park K, Shin H, Choi Y, Yoon JW. Optical energy-difference conservation in a synthetic anti-PT-symmetric system. Phys Rev Lett 2021;127(8):083601.
[22] Longhi S. PT symmetry and antisymmetry by anti-Hermitian wave coupling and nonlinear optical interactions. Opt Lett 2018;43(16):4025–8.

[23] Panasyuk GY, Schotland JC, Markel VA. Classical theory of optical nonlinearity in conducting nanoparticles. Phys Rev Lett 2008;100(4):047402.
[24] Li Y, Peng Y-G, Han L, Miri M-A, Li W, Xiao M, Zhu X-F, Zhao J, Alù A, Fan S, et al. Anti-parity-time symmetry in diffusive systems. Science 2019;364(6436):170–3.
[25] Wu J-H, Artoni M, La Rocca GC. Non-Hermitian degeneracies and unidirectional reflectionless atomic lattices. Phys Rev Lett 2014;113(12):123004.
[26] Peng P, Cao W, Shen C, Qu W, Wen J, Jiang L, Xiao Y. Anti-parity-time symmetry with flying atoms. Nat Phys 2016;12(12):1139–45.
[27] Ge L, Türeci HE. Antisymmetric PT-photonic structures with balanced positive-and negative-index materials. Phys Rev A 2013;88(5):053810.
[28] Bergman A, Duggan R, Sharma K, Tur M, Zadok A, Alù A. Observation of anti-parity-time-symmetry, phase transitions and exceptional points in an optical fibre. Nature Commun 2021;12(1):486.
[29] Konotop VV, Zezyulin DA. Odd-time reversal PT symmetry induced by an anti-PT-symmetric medium. Phys Rev Lett 2018;120(12):123902.
[30] Yang F, Liu Y-C, You L. Anti-PT symmetry in dissipatively coupled optical systems. Phys Rev A 2017;96(5):053845.
[31] Shui T, Yang W-X, Li L, Wang X. Lop-sided Raman-nath diffraction in PT-antisymmetric atomic lattices. Opt Lett 2019;44(8):2089–92.
[32] He Y, Wu J, Hu Y, Zhang J-X, Zhu S-Y. Unidirectional reflectionless anti-parity-time-symmetric photonic lattices of thermal atoms. Phys Rev A 2022;105(4):043712.
[33] Zhang Z, Zhang Y, Sheng J, Yang L, Miri M-A, Christodoulides DN, He B, Zhang Y, Xiao M. Observation of parity-time symmetry in optically induced atomic lattices. Phys Rev Lett 2016;117(12):123601.
[34] Tapar J, Kishen S, Emani NK. Spectral singularities and asymmetric light scattering in PT-symmetric 2D nanoantenna arrays. Opt Lett 2020;45(18):5185–8.
[35] Fleischhauer M, Imamoglu A, Marangos JP. Electromagnetically induced transparency: Optics in coherent media. Rev Modern Phys 2005;77(2):633–73.
[36] Yuan J, Yang W, Jing M, Zhang H, Jiao Y, Li W, Zhang L, Xiao L, Jia S. Quantum sensing of microwave electric fields based on Rydberg atoms. Rep Progr Phys 2023;86(10):106601.
[37] Yuan J, Wang X, Chen G, Wang L, Xiao L, Jia S. High-fidelity frequency converter in high-dimensional spaces. Laser Photonics Rev 2024;2400368.
[38] Ling HY, Li Y-Q, Xiao M. Electromagnetically induced grating: Homogeneously broadened medium. Phys Rev A 1998;57(2):1338.
[39] Yuan J, Wu C, Wang L, Chen G, Jia S. Observation of diffraction pattern in two-dimensional optically induced atomic lattice. Opt Lett 2019;44(17):4123–6.
[40] Zhang Z, Liang S, Septembre I, Yu J, Huang Y, Liu M, Zhang Y, Xiao M, Malpuech G, Solnyshkov D. Non-hermitian delocalization in a two-dimensional photonic quasicrystal. Phys Rev Lett 2024;132(26):263801.
[41] Shui T, Yang W-X, Liu S, Li L, Zhu Z. Asymmetric diffraction by atomic gratings with optical PT symmetry in the Raman-Nath regime. Phys Rev A 2018;97(3):033819.
[42] Liu Y-M, Gao F, Fan C-H, Wu J-H. Asymmetric light diffraction of an atomic grating with PT symmetry. Opt Lett 2017;42(21):4283–6.
[43] Chuang Y-L, Lee R-K, et al. Realization of simultaneously parity-time-symmetric and parity-time-antisymmetric susceptibilities along the longitudinal direction in atomic systems with all optical controls. Opt Express 2018;26(17):21969–78.
[44] Ru R, Li H, Zhang S, Pang H, Pan C, Chen H, Wei D, Gao H, Li F. Non-linear talbot effect in electromagnetically induced optical lattice. Results Phys 2024;60:107697.
[45] Niu F, Zhang H, Yuan J, Xiao L, Jia S, Wang L. Photonic graphene with reconfigurable geometric structures in coherent atomic ensembles. Front Phys 2023;18(5):52304.
[46] Yuan J, Zhang H, Wu C, Wang L, Xiao L, Jia S. Tunable optical vortex array in a two-dimensional electromagnetically induced atomic lattice. Opt Lett 2021;46(17):4184–7.
[47] Yuan J, Zhang H, Wu C, Chen G, Wang L, Xiao L, Jia S. Creation and control of vortex-beam arrays in atomic vapor. Laser Photonics Rev 2023;17(5):2200667.
[48] Abbas M, Khurshid A, Hussain I, et al. Investigation of PT-and PT-antisymmetry in two dimensional (2D) optical lattices. Opt Express 2020;28(6):8003–15.
[49] Wang X, Wu J-H. Optical PT-symmetry and PT-antisymmetry in coherently driven atomic lattices. Opt Express 2016;24(4):4289–98.
[50] Wu J-H, Artoni M, La Rocca GC. Parity-time-antisymmetric atomic lattices without gain. Phys Rev A 2015;91(3):033811.
[51] Yu Q, Yuan J, Liu Z, He R, Liang S, Zhang Y, Zhang Z. Discrete dynamics of light in an anti-parity-time symmetric photonic lattice in atomic vapors. Opt Lett 2023;48(21):5735–8.
[52] Wen F, Ye H, Zhang X, Wang W, Li S, Wang H, Zhang Y, Qiu C-w. Optically induced atomic lattice with tunable near-field and far-field diffraction patterns. Photonics Res 2017;5(6):676–83.